International Journal of Pharmaceutics: X 6 (2023) 100212

Contents lists available at ScienceDirect

International Journal of Pharmaceutics: X

journal homepage: www.sciencedirect.com/journal/international-journal-of-pharmaceutics-x

Impact of mucus modulation by *N*-acetylcysteine on nanoparticle toxicity

Enkeleda Meziu [a,b], Kristela Shehu [a,b], Marcus Koch [a], Marc Schneider [b,*], Annette Kraegeloh [a,*]

[a] *INM – Leibniz Institute for New Materials, 66123 Saarbrücken, Germany*
[b] *Department of Pharmacy, Biopharmaceutics & Pharmaceutical Technology, Saarland University, 66123 Saarbrücken, Germany*

ARTICLE INFO

Keywords:
Calu-3 cells
Polystyrene nanoparticles
Mucus penetration
Cytotoxicity
Air interface culture (AIC)

ABSTRACT

Human respiratory mucus is a biological hydrogel that forms a protective barrier for the underlying epithelium. Modulation of the mucus layer has been employed as a strategy to enhance transmucosal drug carrier transport. However, a drawback of this strategy is a potential reduction of the mucus barrier properties, in particular in situations with an increased exposure to particles. In this study, we investigated the impact of mucus modulation on its protective role. *In vitro* mucus was produced by Calu-3 cells, cultivated at the air-liquid interface for 21 days and used for further testing as formed on top of the cells. Analysis of confocal 3D imaging data revealed that after 21 days Calu-3 cells secrete a mucus layer with a thickness of 24 ± 6 μm. Mucus appeared to restrict penetration of 500 nm carboxyl-modified polystyrene particles to the upper 5–10 μm of the layer. Furthermore, a mucus modulation protocol using aerosolized *N*-acetylcysteine (NAC) was developed. This treatment enhanced the penetration of particles through the mucus down to deeper layers by means of the mucolytic action of NAC. These findings were supported by cytotoxicity data, indicating that intact mucus protects the underlying epithelium from particle-induced effects on membrane integrity. The impact of NAC treatment on the protective properties of mucus was probed by using 50 and 100 nm amine-modified and 50 nm carboxyl-modified polystyrene nanoparticles, respectively. Cytotoxicity was only induced by the amine-modified particles in combination with NAC treatment, implying a reduced protective function of modulated mucus. Overall, our data emphasize the importance of integrating an assessment of the protective function of mucus into the development of therapy approaches involving mucus modulation.

1. Introduction

Human pulmonary mucus is a viscoelastic hydrogel with a complex composition and molecular structure that humidifies, lubricates and protects the underlying airway epithelium (Bansil and Turner, 2018). The primary structural building blocks of mucus are mucin glycoproteins that consist of a protein backbone and oligosaccharide side chains. Mucin terminals contain non-glycosylated cysteine rich domains, which are responsible for disulfide bond formation, and allow the formation of a three-dimensional covalently linked hydrogel. The various regions of mucin molecules show unique properties and interact through hydrophobic, hydrophilic, and electrostatic or specific interactions (Gamazo et al., 2015). Given these structural and chemical properties, mucus traps and removes harmful entities like microbes, pollutants and xenobiotics by adhesive and steric filtering followed by mucociliary clearance (Button et al., 2012). Besides its protective function, mucus represents a selective barrier for transmucosal drug carriers, which need to overcome the mucus layer in order to yield a therapeutic effect. Strategies employed to enhance mucus penetration of drug carriers can broadly be summarized as drug carrier modifications, mucus modulation (by pretreating mucus with a mucus modulating agent) and synergistic combination of both approaches (Chater et al., 2018).

The strategy of mucus modulation is especially relevant in diseases related to hyperconcentrated mucus (*e.g.,* cystic fibrosis, chronic obstructive pulmonary disease). Modulation of mucus can be achieved by various approaches. Main strategies aim at either increasing mucus hydration, breaking covalent interactions between mucins or other mucus macromolecules, and reducing non-covalent interactions

Abbreviations: TEER, transepithelial electrical resistance; SEM, scanning electron microscopy; CLSM, confocal laser scanning microscopy; NAC, *N*-acetylcysteine; PS-NPs, polystyrene nanoparticles; COOH-PS-NPs, carboxyl-modified polystyrene nanoparticles; NH_2-PS-NPs, amine-modified polystyrene nanoparticles; LDH, lactate dehydrogenase; HDMS, hexamethyldisilane; PBS, phosphate-buffered saline; RT, room temperature; WGA-Rhod, wheat germ agglutinin-tetramethyl Rhodamine.

* Corresponding authors.
E-mail addresses: Marc.Schneider@uni-saarland.de (M. Schneider), annette.kraegeloh@leibniz-inm.de (A. Kraegeloh).

https://doi.org/10.1016/j.ijpx.2023.100212
Received 1 March 2023; Received in revised form 14 September 2023; Accepted 17 September 2023
Available online 21 September 2023
2590-1567/© 2023 The Authors. Published by Elsevier B.V. This is an open access article under the CC BY-NC-ND license (http://creativecommons.org/licenses/by-nc-nd/4.0/).

between mucus components (Nordgård and Draget, 2018). Mucolytic agents, of which *N*-acetylcysteine (NAC) is a well-known example, also serve as penetration enhancer for transmucosal drug carriers. Such treatment involves pre- or co-treatment of mucus with the mucolytic agent applied *via* inhalation prior- or simultaneously to the application of the relevant drug carrier (Lababidi et al., 2020; Suk et al., 2011b). The ease of use is one advantage of this technique compared to the challenging large-scale production of surface-modified drug carriers (Chater et al., 2018). While mucus modulation facilitates penetration of drug carriers, it simultaneously compromises its protective function against other inhalable, potentially hazardous materials, including biological particulate matter and abiotic particles, such as cigarette smoke, environmental and anthropogenic fine dust, engineered nanomaterials, advanced materials, and microplastics (Carlson et al., 2018; Vethaak and Legler, 2021; Wu et al., 2018; Xia et al., 2022). Loss of the protective function of mucus and increased vulnerability of the underlying epithelium toward inhalable, potentially hazardous materials is one major concern regarding this strategy (Murgia et al., 2018). Although mucus is considered an efficient barrier against such foreign entities, there is evidence suggesting that for example engineered nanomaterials possess mucus penetrating properties (Jachak et al., 2012). Once the mucus barrier is overcome, these nanoparticles might reach and damage the underlying epithelium (Wang et al., 2011). This risk potentially increases after modulation of mucus, emphasizing the importance to evaluate whether, after modulation, mucus retains its protective function against abiotic particles. The impact of mucus modulation on unintended penetration and subsequent effects of abiotic particles remains poorly investigated.

In this study, the barrier capacity of modulated mucus was probed using model polystyrene nanoparticles. *In vitro* mucus was obtained by cultivating Calu-3 cells at the air liquid interface (Nafee et al., 2018; Sonntag et al., 2022). In the first part, the basic properties of the employed Calu-3 mucus model were monitored regarding integrity of the cellular barrier, cell morphology, mucin production, and mucus layer formation. Secondly, an efficient mucus modulation protocol, comprising pre-treatment of mucus with nebulized *N*-acetylcysteine, was developed. Finally, the protective role of mucus upon modulation was evaluated by microscopy analysis of particle penetration into the mucus and by determining cytotoxicity, induced by polystyrene model nanoparticles.

2. Materials and methods

2.1. Particles and particle characterization

Amine-modified polystyrene nanoparticles (NH_2-PS-NPs) (50 and 100 nm diameter), carboxyl-modified polystyrene nanoparticles (COOH-PS-NPs) (50 nm diameter) obtained from Sigma Aldrich (Steinheim, Germany) and 500 nm (diameter) dragon green-conjugated carboxyl-modified polystyrene particles (COOH-PS-Ps) (Bangs Laboratories, Fisher Scientific, USA) were used for probing the barrier and protective properties of mucus. The average hydrodynamic diameter of the particles was evaluated at 25 °C by dynamic light scattering using a Zetasizer NanoZSP instrument (Malvern Instruments, Worcestershire, UK) (Table 1). Samples were diluted 1:1000 in Dulbecco's phosphate buffered saline (DPBS). A HeNe laser ($\lambda = 633$ nm) was used to irradiate samples and the fluctuating intensity of the scattered light was detected at a backscattering angle of 173°. Measurements were performed in triplicates. The zeta potential of the particles was determined using a Zetasizer NanoZSP instrument (Malvern Instruments, Worcestershire, UK). Samples were diluted 1:9 in 10 mM KCl. Three independent measurements were performed (Table 1).

2.2. Cell culture

Calu-3 (HTB-55™) epithelial cells (Fogh et al., 1977) were obtained from the American Type Culture Collection (ATCC; Rockville, MD, USA) and used as mucus-producing cell model. Cells were maintained in a humidified incubator (37 °C, 5% CO_2, and pH 7.4). Minimal essential medium (MEM) (Gibco Invitrogen, Grand Island, USA) was supplemented with 10% fetal bovine serum (FBS) (PAN-Biotech GmbH, Aidenbach, Germany), 1% sodium pyruvate (Life Technologies, Grand Island, USA), 1% non-essential amino acids (Life Technologies, Grand Island, USA), and 50 U/ml Penicillin and 50 µg/ml Streptomycin (Gibco Invitrogen, Grand Island, USA). Calu-3 cells were sub-cultivated when they attained a confluence of around 70% by firstly washing them with a pre-warmed DPBS (Sigma-Aldrich, Steinheim, Germany) solution. Afterwards, they were trypsinized for 20 min with a 0.05% trypsin solution containing 0.02% EDTA) (PAN Biotech, Aidenbach, Germany).

For mucus production, cells at passage numbers up to 15 were seeded at a density of 10^5 cells/ml in transwell plates with membrane inserts (1.12 cm^2 surface area and 0.4 µm pore size) (Greiner Bio-One GmbH, Frickenhausen, Germany). The plates initially contained 1500 µl medium in the basolateral compartment and 500 µl medium in the apical compartment. Cells were allowed to adhere to the apical transwell membrane covered with medium for 24 h. After removal of the apical medium, the cells were cultivated at air interface culture (AIC) conditions for up to 21 days in order to promote cell differentiation (Haghi et al., 2014). The medium in the basolateral compartment was replaced every other day.

Table 1
Physicochemical properties of particles used in this study.

PS-NPs	Labeling	Hydrodynamic diameter [nm]	Zeta potential [mV]	Experiments
500 nm COOH-PS-Ps	dragon green	452 ± 99	−57	CLSM experiments
50 nm NH_2-PS-NPs	fluorescent blue	42 ± 9	47	LDH assay
100 nm NH_2-PS-NPs	fluorescent orange	70 ± 16	45	LDH assay
50 nm COOH-PS-NPs	–	45 ± 10	−48	LDH assay

2.3. Transepithelial electrical resistance

The formation of a confluent and tight monolayer was monitored by evaluation of Transepithelial Electrical Resistance (TEER) values by using STX-2 electrodes connected to an EVOM™ Epithelial Voltohmmeter (WPI, Sarasota, USA). During assessment of TEER values, 500 µl pre-warmed medium was added to the apical compartment. TEER values were calculated by subtracting the blank values of empty transwell inserts from the measured values of the samples. TEER values of ≥300 Ω cm^2 were considered to indicate the formation of tight cell barriers (Juntke et al., 2021; Nafee et al., 2018).

2.4. Scanning electron microscopy (SEM)

For visualization of the Calu-3 cell surface, mucus was removed by washing the apical compartment with phosphate-buffered saline (PBS). Samples were then fixed with a 2% glutaraldehyde solution for 30 min and dehydrated by incubation in a graded ethanol series (30%–96%, 10 min at each concentration). Subsequently, samples were immersed twice in absolute ethanol for 30 min, in hexamethyldisilazane (HMDS) (Carl Roth, Karlsruhe, Germany) / ethanol (1/1, *v*/v) for 15 min and pure HMDS (twice) for 15 min. Cells were air-dried overnight to allow for evaporation of the organosilicon compound. The filter supporting the Calu-3 cells was separated from the transwell insert. Samples were then

placed on aluminum stubs using double-sided carbon tape. Imaging was carried out using FEI (Hilsboro, Oregon, United States) Quanta 400 FEG in low vacuum mode (100 Pa) using a large field detector (LFD) and acceleration voltages of 5 kV and 10 kV at a working distance of 7.5–13.0 mm.

2.5. Sample preparation for confocal microscopy

Staining of the cellular mucus model: Cell samples were fixed using freshly prepared 4% (*v*/v) paraformaldehyde (Electron microscopy science, Hatfield, UK) and permeabilized with 0.2% Triton-X 100 solution (Carl Roth, Karlsruhe, Germany). Paraformaldehyde as a crosslinking fixative has been used, as it has been described before to successfully preserve mucus structure (Meziu et al., 2021; Hasegawa et al., 2017; Esther et al., 2019). Subsequently, samples were blocked with 5% (*w/v*) bovine serum albumin (Carl Roth, Karlsruhe, Germany). Fluorescence staining for cell junctions, actin, and mucins was performed as follows:

For staining of occludin, after addition of 10 μg/ml mouse anti-occludin primary antibody (Santa Cruz Biotechnology Inc., *CA*. USA), samples were incubated overnight at 4 °C. 10 μg/ml Atto 647 N conjugated anti-mouse secondary antibody (Sigma Aldrich, Steinheim, Germany) was added and incubated for 90 min at room temperature (RT).

Zonula occludens-1 (ZO-1) was stained with 0.625 ng/ml rabbit anti-ZO-1 primary antibody (Life Technologies, Rockville MD, USA) overnight at 4 °C and subsequently with 5 μg/ml Alexa Fluor 488 conjugated anti-rabbit secondary antibody (Sigma Aldrich, Steinheim Germany) overnight at 4 °C.

For staining of E-cadherin, samples were incubated with 10 μg/ml mouse anti-E-cadherin primary antibody (Santa Cruz Biotechnology Inc., CA, USA) overnight at 4 °C and 10 μg/ml Atto 647 N conjugated anti-mouse secondary antibody for 90 min at RT.

For actin staining, samples were incubated with 100 nM phalloidin Atto 647 N (Atto-Tec, Siegen, Germany) for 1 h at RT.

For MUC5B staining, samples were incubated with 2 μg/ml mouse anti-MUC5B primary antibody (Thermo Fisher Scientific, Rockford, USA) for 1 h at RT and 10 μg/ml Atto 647 N conjugated anti-mouse secondary antibody (Sigma Aldrich, Siegen, Germany) for 1 h at RT. MUC5AC was stained using 2 μg/ml rabbit anti-MUC5AC primary antibody (antibodies-online GmbH, Aachen, Germany) for 1 h at RT and 10 μg/ml Alexa Fluor 488 conjugated anti-rabbit secondary antibody (Sigma Aldrich, Steinheim Germany) for 1 h at 4 °C as described before (Meziu et al., 2021). Subsequently, stained samples were embedded in Mowiol 488 (Carl Roth, Karlsruhe, Germany).

Staining of glycoproteins using wheat germ agglutinin: Staining of *in vitro* mucus was performed prior to the evaluation of mucus thickness and for the investigation of particle transport through Calu-3 mucus. The staining agent was applied at the basolateral compartment to avoid mucus dilution. Calu-3 cells were stained with 100 μg/ml wheat germ agglutinin-tetramethyl Rhodamine (WGA-Rhod) (Vector Laboratories Inc., CA, USA) for 2 h at 37 °C. The treatment also results in staining of intracellular and membrane bound glycoproteins. Nevertheless, the staining allowed for a morphological discrimination between mucus and cell layer (Supplementary information, Fig. S1). Prior to imaging, the membranes including the attached Calu-3 cells were separated from the transwell insert and placed on an Ibidi® imaging dish with a coverslip bottom.

2.6. Confocal laser scanning microscopy (CLSM)

Samples were examined with a TCS-SP5 STED setup (Leica Microsystems, Mannheim, Germany), in confocal mode, using the oil immersion objectives 63×/1.4 and 100×/1.4 (HCX PL APO). The fluorescent dyes Alexa 488 and Dragon Green were excited using the 488 nm laser line of an argon laser (λ = 488 nm). Atto 647 N and rhodamine were excited using a HeNe laser (λ = 633 nm), and a DPSS laser (λ = 561 nm) respectively. The fluorescence signals were detected using a photomultiplier. For analysis of mucus thickness and particle penetration, z stacks (step size 1 μm) of the samples were recorded. To allow for quantitation of the intensities between different images, the settings for image acquisition were kept constant.

2.7. Image processing

For the quantification of particle transport across mucus, the raw fluorescence intensity of the particle signals in the obtained z-stacks was quantitatively analyzed using *Image J* software, version 1.53e. For analysis of mucus thickness, the recorded z-stacks were reconstructed using *Image J* software and analyzed to determine the distance between the outermost mucus layer and cell layer (mucus thickness).

2.8. Exposure of Calu-3 cells to aerosols using Vitrocell® Cloud 6

Calu-3 cells grown under AIC were exposed to NAC and/or polystyrene particles using the Vitrocell® Cloud 6 system (VITROCELL Systems GmbH, Waldkirch, Germany). NAC, particles, and NaCl were nebulized using an Aerogen Pro vibrating mesh nebulizer (Aerogen Ltd. Galway, Ireland) (nominal average droplet size range 4 μm). The nebulized doses were monitored with the integrated quartz crystal microbalance (Ding et al., 2020).

To analyze particle penetration, cell samples were stained with WGA-Rhod as described in Section 2.5., prior to particle treatment. Subsequently, samples were exposed to 200 μl of 500 nm dragon green-labeled COOH-PS-Ps at a particle concentration (solid content) of 10 mg/ml. Samples were incubated for 3 h at 37 °C prior to microscopy analysis.

For treatment of cell samples with NAC, a solution of 20% NAC (Pharmazell GmbH, Barsbüttel, Germany) in 0.9% NaCl (Carl Roth GmbH, Karlsruhe, Germany) at pH 7.5 was prepared. (Suk et al., 2011a). The dose of NAC to be deposited during the experiments, was estimated by considering the clinical dose (3–5 ml of 20% (*w/v*) NAC solution given 3–4 times/day), the tracheobronchial surface area (2471 cm^2) (Jachak et al., 2012), and the deposition factor (percentage of the applied dose that reaches the respiratory tract) (10%) (Carvalho et al., 2011; Tseng et al., 2022). Based on this approach, 120 μg/cm^2 NAC was calculated to be deposited onto the tracheobronchial surface per day during clinical use. In this study, the impact of NAC on particle penetration was investigated using two doses: 20 μg/cm^2 NAC, approximating the lowest amount of NAC delivered by a single administration and 120 μg/cm^2 NAC, approximating the maximum cumulative daily dose of NAC during pulmonary administration. NAC treated samples were incubated for 30 min at 37 °C as suggested by (Suk et al., 2011a) prior to application of polystyrene particles. 0.9% NaCl was used as vehicle control and applied at corresponding volumes.

For evaluation of particle induced cytotoxicity, Calu-3 cells were exposed to 25 μg/cm^2, 50 μg/cm^2, and 100 μg/cm^2 of NH_2-PS-NPs with a diameter of 50 nm and 100 nm and COOH-PS-NPs with a diameter of 50 nm, respectively. Cells were then incubated for 24 h at 37 °C prior to performing the cytotoxicity assay.

2.9. Membrane integrity assay

After exposure of Calu-3 cells to NPs as described in Section 2.8, membrane integrity was determined based on the activity of lactate dehydrogenase (LDH) in the cell culture medium. The CytoTox-ONE Homogeneous Membrane Integrity Assay (Promega GmbH, Walldorf, Germany) was used according to the manufacturer's instructions. In brief, 100 μl basolateral medium was removed, mixed with an equal volume of the assay reagent and incubated for 10 min at RT in the dark. After adding 50 μl of stop solution, fluorescence was recorded with a Tecan microplate reader (Tecan Trading AG, Männedorf, Switzerland) at an excitation wavelength of 560 nm and an emission wavelength of 590 nm. Background fluorescence of cell-free medium was subtracted from

the recorded values. Membrane integrity was determined relative to a positive control (cells treated with 9% Triton X100).

3. Results and discussion

3.1. Calu-3 cells at the air interface represent an adequate in vitro model for conducting mucus research

Calu-3 cells, cultivated at the air interface, are a highly useful cellular mucus model for the investigation of delivery systems intended for pulmonary use (Sonntag et al., 2022). Commercial availability and tight junction formation are the advantages of the Calu-3 cell line as an *in vitro* model (Braakhuis et al., 2023). In particular, mucus production when cultured at air interface conditions, is an important benefit of the use of Calu-3 cell line, compared to other commonly used airway epithelium cell lines (Ghanem et al., 2021).

However, the mucin expression profile is another important mucus property. MUC5AC and MUC5B are the main mucins of airway mucus (Sonntag et al., 2022). MUC5B has been described as predominant mucin (Song et al., 2022) in the healthy and the diseased state. In comparison, Calu-3 cells secrete MUC5AC over MUC5B (Berger et al., 1999). However, this cell line has been used for particle penetration studies independent of a specific disease (Nafee et al., 2018; Sonntag et al., 2022).

In vitro mucus, when used as formed on top of the cells, is beneficial as it cannot only be used for penetration studies, but also allows for monitoring cellular responses. However, the characterization of such models in terms of mucus and mucin concentration is challenging, first of all due to formation of very low amounts of mucus especially after short cultivation times. Furthermore, mucus volume and concentration might be altered during mucus collection, especially, when washing steps are involved. Mucus concentration is defined as dry to wet weight content (% solids content), mucin concentration describes the absolute mucin concentration (Henderson et al., 2014; Hill et al., 2014; Boucher, 2019). Relating *in vitro* mucus properties to any specific physiological or pathological situation is limited by availability of quantitative information regarding mucus concentration under these conditions. In the frame of this study, *in vitro* mucus was produced by Calu-3 cells cultured at air interface conditions. Therefore, the properties of Calu-3 cells as an *in vitro* airway epithelial model for conducting mucus research were assessed in terms of barrier properties, morphology, and mucin production. The barrier properties of Calu-3 cells were evaluated by measurement of the TEER values combined with microscopy detection of protein structures characteristic for tight junctions. After 10 days, cells cultivated at air interface conditions exhibited TEER values $\geq$300 Ω cm^2 (Fig. 1 A), confirming the formation of an intact barrier (Mura et al., 2011). Previous studies report inconsistent data regarding the required culture conditions (submerse *vs.* AIC) and duration (varying between 5 up to 16 days) to achieve TEER values, which are regarded as representative (Grainger et al., 2006; Haghi et al., 2014; Stentebjerg-Andersen et al., 2011). This emphasizes the importance of TEER value assessment. Barrier integrity of Calu-3 cells was further assessed by staining and visualizing cellular junctions. CLSM images confirmed the presence of occludin, ZO-1 and E-cadherin (Fig. 1 B—D). These data are consistent with previous studies, reporting on tight junction formation in Calu-3 cells (Kreft et al., 2015; Wan et al., 2000).

SEM images of Calu-3 cells maintained at AIC revealed a heterogeneous population of apically located cellular protrusions (Fig. 2 A-B). Such protrusions have been previously described as cilia (motility structures, containing microtubules) or microvilli (supported by actin) (Florea et al., 2003; Kreft et al., 2015; Osinka et al., 2019; Tilney et al., 2004). In this study, imaging of phalloidin labeled samples confirmed that the protrusions are actin-associated and therefore can be regarded as microvilli (Fig. 2 C—D).

Furthermore, the mucin secreting activity of Calu-3 cells was investigated, focusing on the two major gel-forming mucins of conducting airways, MUC5AC and MUC5B. CLSM sections recorded in the extracellular mucus layer covering Calu-3 cells revealed the presence of both MUC5B and MUC5AC (Fig. 3 A and B). The overlay (Fig. 3 C) revealed that in this layer, the mucins are not homogeneously distributed. Rather, regions predominantly containing MUC5AC or MUC5B or regions containing a mixture of both mucins could be differentiated.

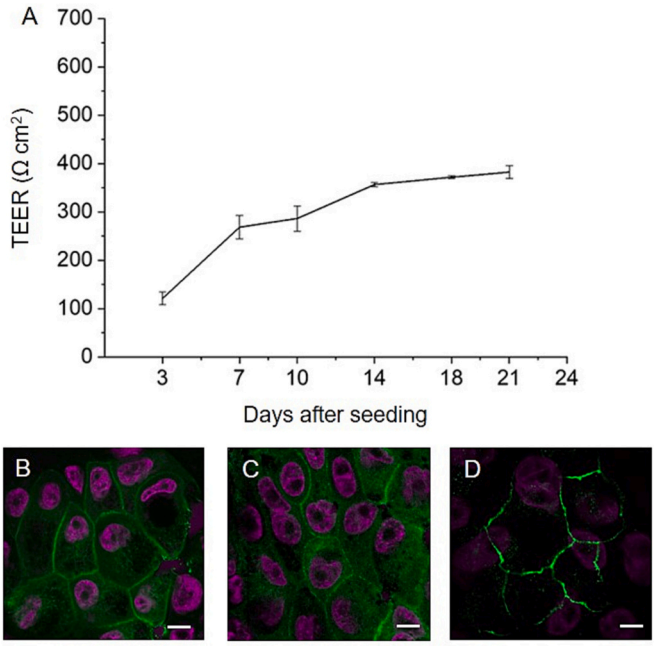

Fig. 1. Development of barrier properties during cultivation of Calu-3 cells at the air-liquid interface for up to 21 days. A) TEER values indicate the formation of a tight monolayer ($\geq$ 300 Ω cm^2) starting from day 14. Data shown are mean values ± SE for n = 27 from 3 independent experiments. B—D) Expression of occludin (green) E-cadherin (green) and ZO-1 (green). Scale bar 10 μm. (For interpretation of the references to colour in this figure legend, the reader is referred to the web version of this article.)

CLSM sections through the cells revealed that the mucins MUC5AC and MUC5B are intracellularly located within round shaped structures, indicating their presence inside of membrane-bound vesicles (Fig. 3 D and E) also called granules (Lillehoj et al., 2013). Again, the mucins appear to be unevenly distributed within the vesicles (Fig. 3 F). Several gene expression studies have reported the expression of both MUC5AC and MUC5B in Calu-3 cells (Gupta et al., 2019; Lee et al., 2021). Sonntag et al. (2022) assessed mucus production in Calu-3 cells by evaluating the level of MUC5AC formation. Analyses based on immunofluorescence staining also confirmed the formation of MUC5AC and MUC5B by Calu-3 cells (Lodes et al., 2020). However, the ultrastructure of intracellular MUC5B and MUC5AC filled-granules and the resulting morphology of the mucus layer secreted by Calu-3 cells have previously been poorly addressed. Previous immunohistochemical studies found MUC5AC filled intracellular secretory granules residing at the apical side of Calu-3 cells, grown at the air interface (Kreda et al., 2007; Meindl et al., 2015). In general, goblet cells are polarized. The nucleus and organelles are reported to reside at the base of the cell, whereas the mucin-secreting vesicles accumulate at the apical side (Bustamante-Marin and Ostrowski, 2017).

Tight junction formation resulting in generation of physiological TEER values together with the secretion of the major gel forming mucins confirmed the quality and adequacy of the employed Calu-3 model for conducting this study.

3.2. N-acetylcysteine improves particle penetration

NAC has mucolytic, antioxidant (ROS scavenging), and anti-

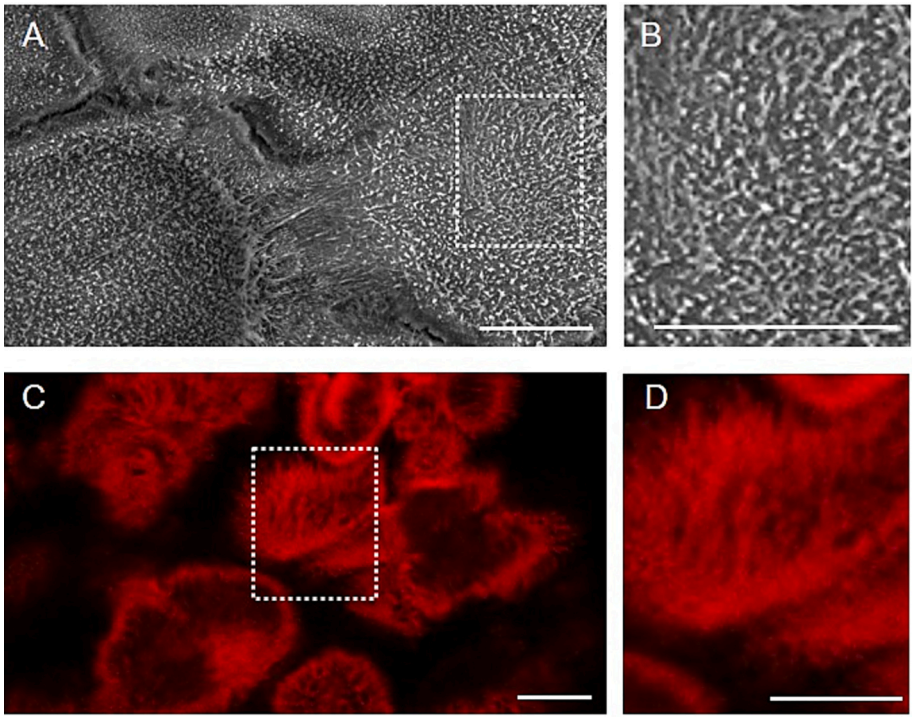

Fig. 2. Protrusions at the apical surface of Calu-3 cells exposed to AIC conditions. A) SEM images show short protrusions in the middle of the cells and longer protrusions at the cell edges. B) Enlarged image of the area denoted with the dashed box in A. C) CLSM images of Calu-3 cells stained for actin with phalloidin Atto 647. D) Enlarged image of the area denoted with the dashed box in C. Scale bar 10 μm.

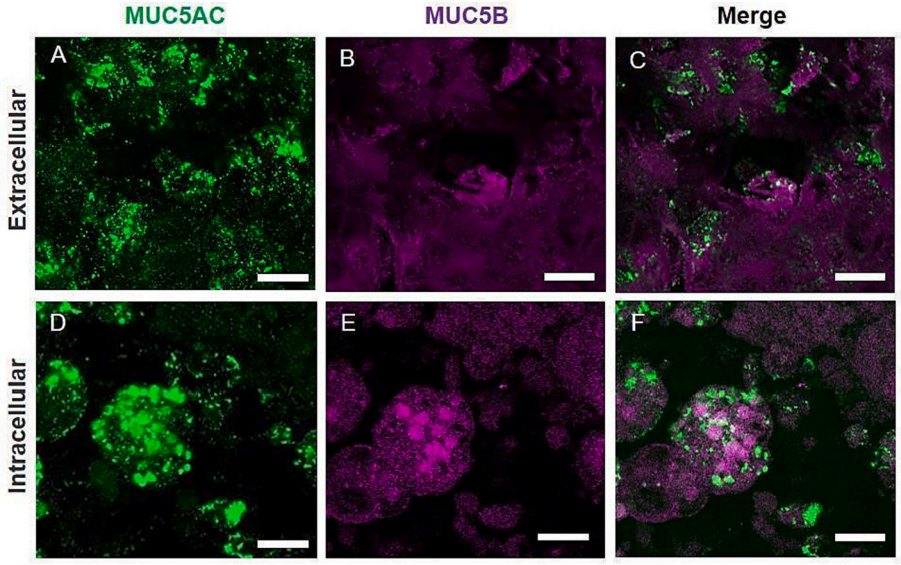

Fig. 3. Calu-3 cells cultured under AIC conditions secrete the major gel forming mucins MUC5AC and MUC5B. A-C) 2D sections taken above the cells demonstrate the secretion of both MUC5AC and MUC5B. D-E) 2D sections through the cells show the presence of MUC5AC and MUC5B filled granules. Samples were stained with anti-MUC5AC Alexa Fluor 488 (green) and anti-MUC5B-Atto 647 N (magenta). Scale bar 10 μm. (For interpretation of the references to colour in this figure legend, the reader is referred to the web version of this article.)

inflammatory properties (Frye and Berk, 2018). Given these properties, nebulized NAC has been clinically used in acute and chronic broncho-pulmonary diseases that are associated with impaired mucus formation and transport (Calverley et al., 2021). However, its use as a mucus modulator with the scope of improving the diffusion of particulate based therapeutics (Suk et al., 2011b) is yet a subject of ongoing research (Chater et al., 2018).

As a proof of concept, we investigated how pretreatment of mucus with nebulized NAC influenced the penetration behavior of 500 nm model COOH-PS-Ps through *in vitro* mucus. Particles larger than 200 nm have been described not to penetrate mucus (Murgia et al., 2016). Therefore, the 500 nm particles were chosen here as a control, allowing to show the mucus penetration enhancing effect of NAC. Pharmaceutical aspects such as high drug encapsulation efficiency and modifiable drug release kinetics are other considerations that in general foster the use of sub-micrometer to micrometer-sized particles in the field of formulation

development (Suk et al., 2011b).

For bearing resemblance to the treatment situation, the exposure of Calu-3 cells to NAC and PS-NPs was performed using the Vitrocell ® Cloud system. NAC solution was nebulized and administered at doses of 20 μg/cm^2 ± 10% and 120 μg/cm^2 ± 10%. 3 h after particle application, 2D images were recorded at different optical z-sections starting from the top of the mucus layer (Supplementary information, Fig. S2) of the samples as illustrated in Fig. 4. The presence of particles was quantified (Fig. 5) based on fluorescence intensity and using *Image J* software.

In untreated samples, the 500 nm particles were only detected in the upper mucus layers. Signal intensity was highest at the top layer (0 μm) and decreased with increasing distance from the top. At distances of 15 μm and more, particles were only detected occasionally, even after 3 h of incubation (Fig. 4). The impact of 0.9% NaCl, used as vehicle control for NAC, on the penetration of particles appeared to be negligible. Samples pretreated with NaCl did not exhibit particle penetration to more distant layers as compared to untreated samples (Supplementary information, Fig. S3). These results are in line with previous studies that reported a strong obstruction of 500 nm COOH-PS-Ps to diffuse through mucus (Huck et al., 2019; Murgia et al., 2016). These data reveal that in its untreated state Calu-3 mucus shows considerable barrier properties and represents a promising mucus model for the investigation of mucus drug carrier interactions.

After pretreatment of the samples with 20 μg/cm^2 NAC, according to the quantitative analysis (Fig. 5), no significant increase in particle penetration as compared to the untreated controls was detected. Under these conditions only a few more particle signals were detected at distances of 10 μm and 15 μm (Fig. 4). In contrast, pretreatment of mucus with 120 μg/cm^2 NAC notably improved particle diffusion across mucus (Fig. 5). Here, particles were detected up to a depth of 20 μm (Fig. 4). In addition, the chain-like pattern of particles observed after pretreatment with 120 μg/cm2 NAC (Fig. 4) might indicate the presence of connections between the interstitial fluid-filled regions, accessible to the particles, as already observed before (Nafee et al., 2018). The enhanced nanoparticle diffusivity mediated by NAC can be attributed to an increase of these accessible fluid-filled areas, most likely mediated by the mucolytic properties of NAC. The latter have been described to be based on depolymerisation of the mucin matrix by lysis of interconnecting disulfide bonds (Sadowska, 2012). Ehre et al. (2019) reported that NAC leads to decrease of the molecular weight of mucins, however with a lower efficiency as compared to other novel mucolytics.

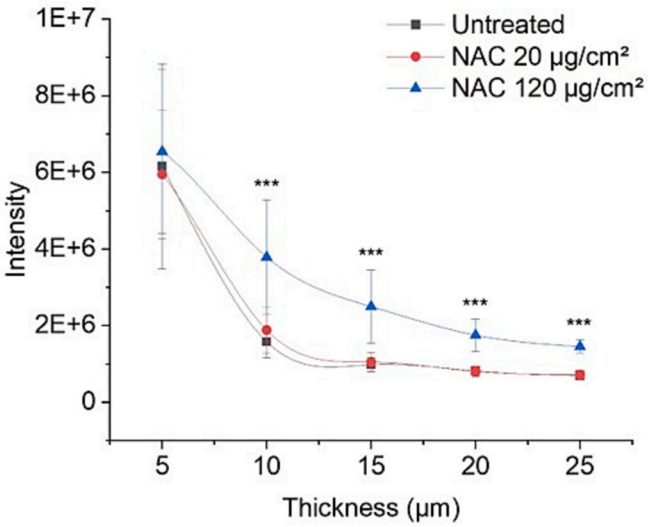

Fig. 5. Quantitative analysis of 500 nm particle penetration after NAC treatment based on confocal imaging. Data shown are mean values ± SE for $n = 9$ sample areas from 3 independent experiments. Statistical significance was calculated with One Way ANOVA followed by the Bonferroni Test and indicated by asterisks: ***, $p < 0.001$.

An increase of the mucus "mesh size" has also been suggested as an explanation for the improvement of nanoparticle transport after NAC treatment, based on SEM imaging (Suk et al., 2011a). However, care should be taken with the interpretation of such observations, as dehydration of samples for SEM imaging has been shown to cause structural alterations of mucus, resulting in the formation of μm-sized pores absent from the hydrated state (Meziu et al., 2021; Kirch et al., 2012; Boegh et al., 2013).

Measurement of the osmolality of 20% NAC solution revealed that it

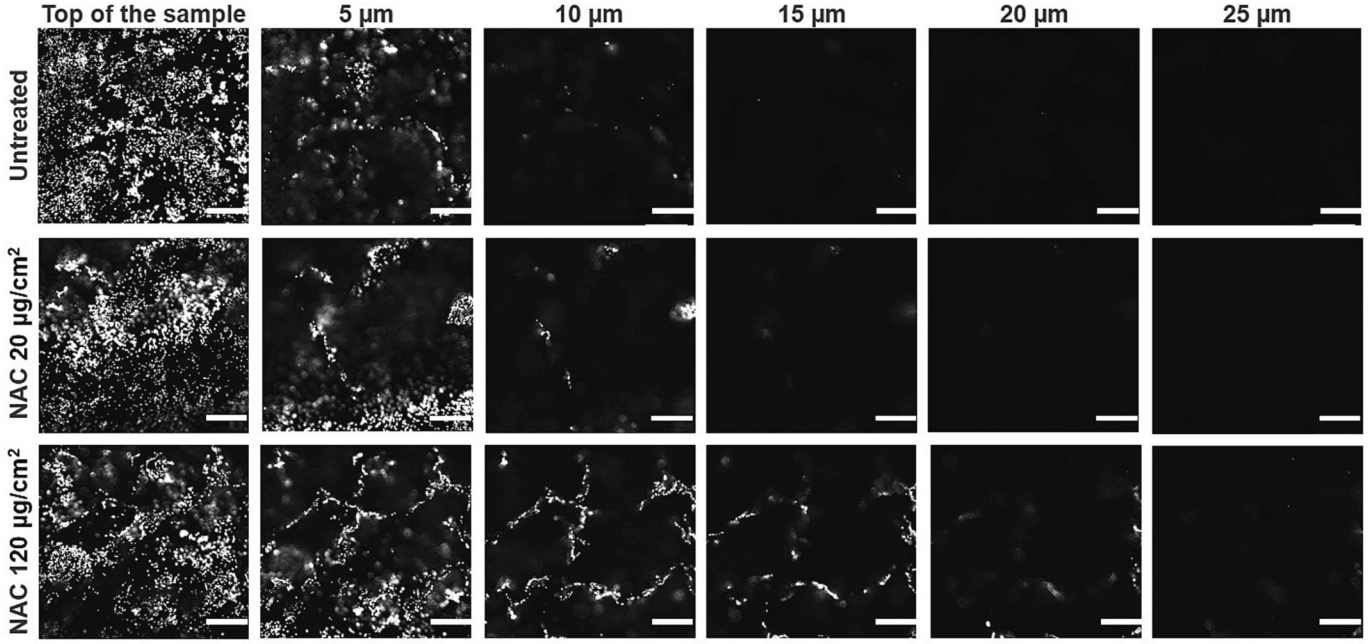

Fig. 4. NAC treatment improves particle penetration into mucus. 2D CLSM images of 500 nm COOH-PS-Ps (white) at different depths of the mucus: 0 μm represents the top of the sample, 25 μm represents the bottom layer. Mucus was untreated (top row) or treated with 20 μg/cm^2 NAC (middle) and 120 μg/cm^2 NAC (bottom row), respectively. Particles and NAC were applied to the top of the sample. Scale bar 50 μm.

is a hypertonic solution with an osmolality equivalent to 4.5% NaCl (Supplementary information, Table 1). Application of 20% NAC solution therefore might also act as osmolyte, causing water influx into the mucus layer and thereby facilitating nanoparticle transport. To differentiate between the mucolytic and osmotic effect of NAC, Calu-3 cells, cultured for 21 days, were pretreated with 4.5% NaCl and 20% NAC. Subsequently, the transport of 500 nm COOH-PS-Ps in untreated, 4.5% NaCl treated, and 20% NAC treated samples was evaluated. Treatment with 4.5% hypertonic NaCl solution did not lead to a significant increase of nanoparticle transport compared to untreated controls (Supplementary information, Fig. S4). This indicates that the mucolytic effect of 20% NAC is dominating over the osmotic or dilution effect. Given the established strong inverse proportionality of mucus viscoelasticity and particle diffusivity, the decrease of complex mucus viscoelasticity (Vukosavljevic et al., 2017) *via* reduction of disulfide bonds by NAC, is most likely the key factor in the enhancement of particle diffusivity (Lababidi et al., 2019; Peng et al., 2021).

The quantitative image analysis confirmed that pretreatment of mucus with a 120 μg/cm^2 dose of NAC significantly increased the penetration of 500 nm COOH-PS-Ps. This behavior was observable from a visualization depth of ≥5 μm compared to untreated samples and samples pretreated with only 20 μg/cm^2 NAC (Fig. 5). NAC treatment did also increase the penetration of 50 nm and 100 nm nanoparticles, as further described in Section 3.5. Different to our findings, Suk et al. reported that the treatment of cystic fibrosis sputum with NAC at a concentration of 20 mM provided almost no improvement for 500 nm COOH-PS-Ps compared to untreated samples. The reasons for this difference may be the even higher viscoelasticity of cystic fibrosis mucus and the pathology-related increased mucin concentration (Morrison et al., 2019) of the used samples, as the NAC induced nanoparticle transport improvement is reported to be inversely correlated to mucin concentration (Suk et al., 2011b).

Taken together, these data provide evidence that the NAC treatment protocol, proposed in this study, can substantially enhance the permeability of mucus and improve nanoparticle transport, indicating a reduced protective effect during such a treatment phase.

3.3. Time dependent formation of in vitro mucus

It has been reported that Calu-3 cells cultivated at air-interface conditions show a time-dependent mucus secretion (Haghi et al., 2014). In the frame of this study, the time-dependent secretion of mucus and build-up of a mucus layer was investigated. Considering the protective function of mucus, the thickness of a complete mucus layer equals the distance that delivery systems as well as potentially hazardous materials must travel to reach the underlying cells. Therefore, the thickness of the mucus layer was assessed by CLSM, after Calu-3 cells were cultivated at air interface conditions for 5 days (Calu-3 5-d) and 21 days (Calu-3 21-d).

In order to avoid removal of loosely bound mucus mediated by washing steps, mucus was stained *via* application of labeled WGA to the basolateral compartment of the transwell filters. The membranes including the attached Calu-3 cells were separated from the transwell insert and placed on an Ibidi® imaging chamber for analysis (Fig. 6 A). Morphological differences were used as a discrimination tool between the cells and the mucus layer (Fig. 6 B). In contrast to previous studies, describing mucus as an even layer (Fiegel et al., 2003), it was observed that the thickness of mucus was not uniform throughout the samples.

However, after 21 days, Calu-3 cells produced a confluent mucus layer (Supplementary information, Fig. S5). Overall, the data indicated a significant increase of the mucus thickness over time (from 5 to 21 days). Calu-3 5d produced a mucus layer of 8.7 ± 4.5 μm, while Calu-3 21d produced a 2.8-fold thicker mucus layer of 24.1 ± 5.8 (Fig. 6 C).

In comparison, Sonntag et al. (2022) reported formation of an approximately 20 μm thick mucus layer by Calu-3 cells after 14 days, however no data was reported for longer cultivation times. The mucus thickness determined in this study after 21 days correlated well with the thickness of human tracheal mucus (10–30 μm) corresponding to the airway generation 0 (Patton, 1996; Wine, 1999). For the subsequent assessment of the protective properties of mucus, Calu-3 cells were used after 5d and 21d of cultivation. For this assessment, a model exhibiting a confluent cell layer and exhibiting barrier properties, while completely lacking a mucus cover would have been the ideal negative control. After 5 days, the cell layer already was confluent (Supplementary information, Fig. S6), whereas TEER values indicated incomplete barrier formation (Fig. 1). However, as the cells were already covered by mucus after 5 days (Supplementary information, Fig. S7), the 5d model was chosen to mimic the protective function of a thin mucus layer on top of confluent cells.

3.4. Protective role of in vitro mucus

To evaluate the protective function of mucus, Calu-3 cells were exposed to three types of model polystyrene nanoparticles. 50 nm and

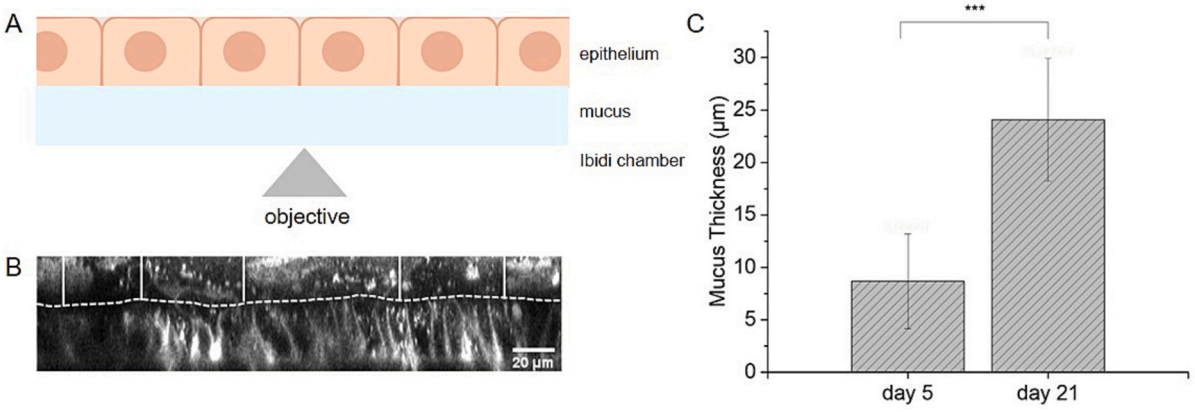

Fig. 6. Thickness of *in vitro* mucus produced by Calu-3 cells increased with culturing time. A) Illustration of the applied CLSM imaging setup. B) Orthogonal view (xz) of mucus covering the epithelium reveals the morphological discrimination between the epithelium below the dashed line and mucus layer on top of the dashed line. *Z*-stacks of 2D images were analyzed using *Image J* to determine mucus thickness (distance between the top layer of mucus and the cell membrane). Mucus thickness was measured at five random spots (white lines) in each sample. Solid white lines represent mucus thickness at arbitrarily chosen locations. Note that the image in B) is rotated 180° as compared to A). C) Average thickness of *in vitro* mucus evaluated after cultivation of Calu-3 cells for 5 and 21 days. Data shown represent mean values ± SE for $n = 45$ measurements from 3 independent experiments. Statistical significance is calculated with One Way ANOVA followed by the Bonferroni Test and indicated by asterisks: ***, $p < 0.001$.

100 nm NH_2-PS-NPs and 50 nm COOH-PS-NPs (Table 1) were applied at varying doses (25, 50 and 100 μg/cm^2). Polystyrene nanoparticles have been intensively used as model particles in the field of drug delivery (Wang et al., 2017), but also for nanotoxicity studies (Walczak et al., 2015). Due to the growing interest in the effects of nano- and microplastics and the potential formation of polystyrene particles due to plastic fragmentation, PS-NPs have also been used in terms of environmental/occupational exposure to these materials (Kik et al., 2020).

For the assessment of nanoparticle induced cytotoxicity, the lactate dehydrogenase (LDH) based membrane integrity assay was performed. For the assay, the nanoparticles were applied *via* nebulization to the apical compartment and the medium samples were taken from the basal compartment. Due to limited translocation of the particles across the transwell membranes, as shown by Dekali et al. (2014), using an acellular translocation assay, significant (optical) interference of the particles with the assay readout can be neglected. Using this assay, cytotoxicity values of ≤20%, correlating with a low release of LDH, are considered nontoxic (López-García et al., 2014).

50 nm NH_2-PS-NPs applied at a dose of 25 μg/cm^2 induced no toxicity in Calu-3 5d and Calu-3 21d samples (Fig. 7 A). At higher doses 50 and 100 μg/cm^2 50 nm NH_2-PS-NPs induced a dose-dependent cytotoxicity in both Calu-3 5d and 21d samples. 50 nm NH_2-PS-NPs induced in Calu-3 5d samples a significantly higher cytotoxicity than in Calu-3 21d.

100 nm NH_2-PS-NPs probed in Calu-3 5-d induced no cytotoxicity at a dose of 25 μg/cm^2 and a dose dependent cytotoxicity at doses of 50 and 100 μg/cm^2 (Fig. 7 B). In samples with a thicker mucus layer Calu-3 21-d 100 nm NH_2-PS-NPs induced no toxicity for all applied concentrations. As in the literature described (Li et al., 2022), the cytotoxicity induced by 50 nm NH_2-PS-NPs was observed to be higher than that of larger 100 nm NH_2-PS-NPs (Fig. 7A-B).

50 nm COOH-PS-NPs induced cytotoxicity only when applied at doses of 50 and 100 μg/cm^2 in Calu-3 5-d samples Fig. 7 C). As previously reported (Dausend et al., 2008) the negatively charged 50 nm COOH-PS-NPs induced a lower cytotoxicity than positively charged 50 nm NH_2-PS-NPs (Fig. 7 B—C).

The nanoparticle induced cytotoxicity was found to be dose dependent for all three nanoparticle types used and both models, Calu-3 cells cultured for 5 and 21 days (Fig. 7 A-C). However, at the lowest dose used, 25 μg/cm^2, the nanoparticles did not induce cytotoxicity. These findings confirm previous results, reporting that the toxicity of nanoparticles increases with increasing concentration (Najahi-Missaoui et al., 2021).

Furthermore, the nanoparticle induced cytotoxicity was more pronounced in case of the Calu-3 5-d samples as compared to the Calu-3 21-d samples (Fig. 7 A-C). These data indicated that Calu-3 5-d are more vulnerable to nanoparticle-induced cytotoxicity as compared to Calu-3 21-d.

Given the mucus thickness difference between Calu-3 5-d and 21-d, the lower nanoparticle-induced toxicity values observed in Calu-3 21-d are most likely attributed to the thick mucus layer and underline the protective function of mucus.

These results indicate that Calu-3 cells cultured at air interface conditions for 21 days secrete a mucus layer of a thickness comparable to the human tracheal mucus that protects the underlying cells and can successfully be employed for the investigation of the impact of NAC on the protective role of mucus.

3.5. NAC modulation of mucus increases nanoparticle-induced cytotoxicity

A considerable concern about the increase of mucus permeability *via* NAC treatment is the vulnerability of the underlying epithelium toward inhalable xenobiotics. In this study, we address this question by probing the impact of NAC treatment on the protective role of mucus using nebulized model PS-NPs. Initial experiments were performed, in order to exclude that NAC itself induced cytotoxicity (Supplementary information, Fig. S8). 50 nm NH_2-PS-NPs applied at a dose of 25 μg/cm^2 did not induce cytotoxicity, independent from any pretreatment with NAC. At higher doses (50 and 100 μg/cm^2) 50 nm NH_2-PS-NPs induced cytotoxicity in both NAC treated and untreated samples. Furthermore, the cytotoxic effect of the 50 nm NH_2-PS-NPs particles was more pronounced after NAC treatment (Fig. 8 A). 100 nm NH_2-PS-NPs induced no

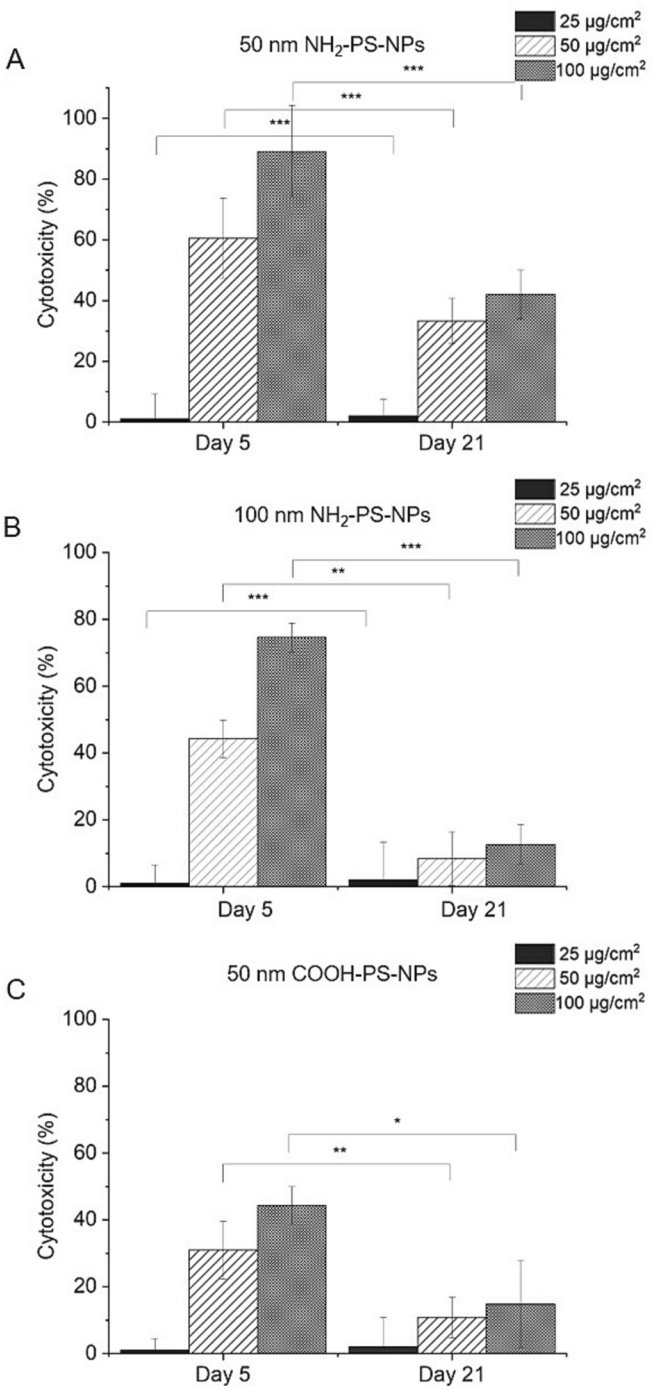

Fig. 7. The protective function of mucus is determined by the thickness of the mucus layer. Samples were exposed to nebulized particles A) 50 nm NH_2-PS-NPs, B) 100 nm NH_2-PS-NPs and C) 50 nm COOH-PS-NPs at three different doses 25, 50, and 100 μg/cm^2. Data shown are mean values ± SE for n = 27 technical replicates from 3 independent experiments. Statistical significance is calculated with one-way ANOVA followed by the Bonferroni Test and indicated by asterisks: *, $p < 0.05$; **, $p < 0.01$; ***, $p < 0.001$.

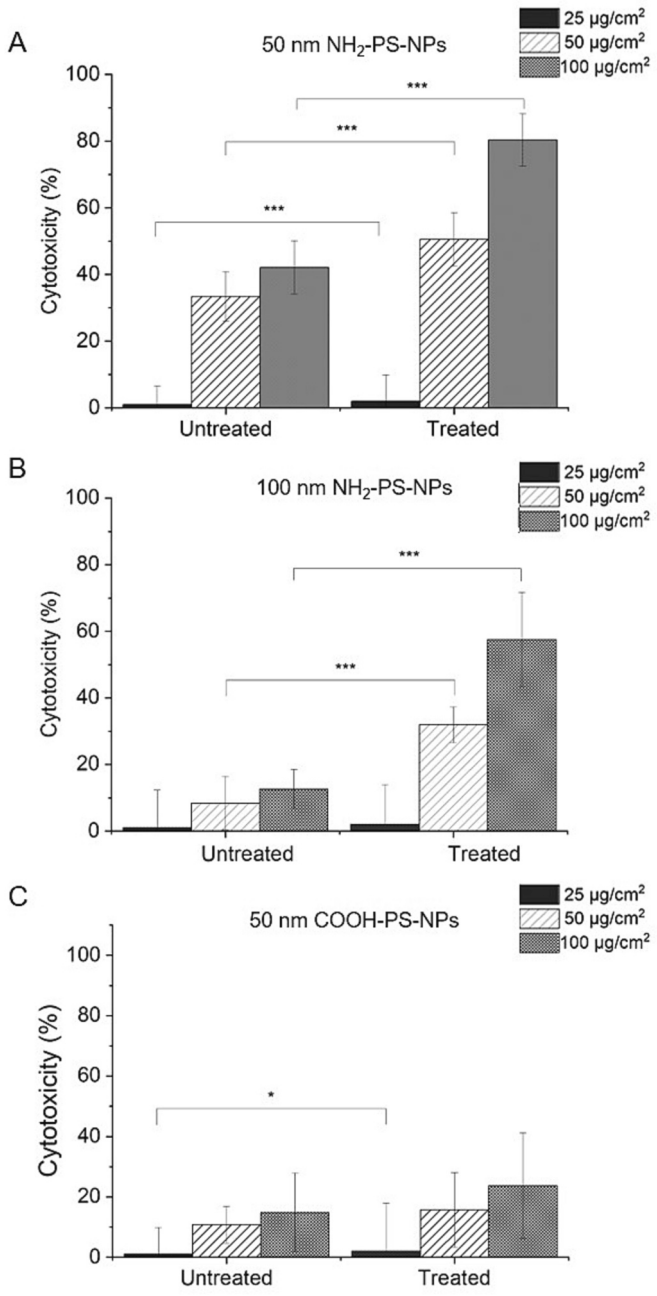

Fig. 8. Pretreatment with NAC decreases the protective function of mucus. Treated samples were exposed to nebulized NAC (120 µg/cm^2). Both treated and untreated samples were subsequently exposed to nebulized particles A) 50 nm NH_2–PS-NPs, B) 100 nm NH_2–PS-NPs and C) 50 nm COOH-PS-NPs at three different doses 25, 50, and 100 µg/cm^2. Data shown are mean values ± SE for n = 27 technical replicates from 3 independent experiments. Statistical significance is calculated with one-way ANOVA followed by the Bonferroni Test and indicated by asterisks: *, $p < 0.05$; **, $p < 0.01$; ***, $p < 0.001$.

toxicity in absence of NAC, independent on the applied dose. After NAC treatment, the 100 nm NH_2-PS-NPs induced toxicity, which was observed to increase with the applied dose (Fig. 8 B). In comparison, 50 nm COOH-PS-NPs induced only slight effects, even when applied after NAC treatment at a dose of 100 µg/cm^2 (Fig. 8 C).

Consistent with the existing literature, it was observed that exposure of cells to particles of smaller diameter and of positive charge caused a more pronounced cytotoxicity (Fröhlich, 2012). Most importantly, NAC-treatment increased the cytotoxicity induced by all particle types as compared to untreated samples (Fig. 8 A-C). In particular, NAC treatment led to an increase in the cytotoxicity of 50 nm and 100 nm NH_2-PS-NPs (Fig. 8 A, B).

NAC is a well-known antioxidant and shows its antioxidant effect *via* various mechanisms. It plays a role as a cysteine and thereby glutathione precursor (a well-known direct antioxidant and a substrate of several antioxidant enzymes), acts as a direct antioxidant, and is assumed to be involved in thiol-disulfide interchange reactions, involved in restoration of thiol pools (Aldini et al., 2018; Ehre et al., 2019). Having this in mind, NAC is expected to attenuate stressor induced oxidative stress due to its antioxidative properties. As polystyrene nanoparticle induced toxicity might be mediated by oxidative stress (Fu et al., 2022), NAC is expected to rather mitigate any nanoparticle induced toxicity. Given the nanoparticle penetration enhancing property of NAC, the increased cytotoxicity values observed after NAC treatment might rather be attributed to an elevated exposure of cells to an increased number of particles. Enhanced nanoparticle induced cytotoxicity observed for the NAC-treated samples suggests that NAC compromises the mucus barrier integrity and its protective function.

Therefore, the impact of NAC treatment on the penetration of nanoparticles was analyzed as described for the 500 nm particles. After 3 h, 100 nm NH_2-PS-NPs did not evenly distribute in the mucus. The fluorescence signals were predominately detected in the top layers. NAC treatment appeared to increase the presence of 100 nm NH_2-PS-NPs particles, even at deeper mucus layers (Supplementary information, Fig. S9). In comparison, 50 nm COOH-PS-NPs (FluoSpheres), even without previous NAC treatment, seemed to distribute more evenly across the mucus and to penetrate deeper in the mucus layers. Nevertheless, NAC treatment appeared to also enhance the penetration of these particles into deeper mucus layers (Supplementary information, Fig. S10).

The observed results are in good agreement with Takatsuka et al., addressing the impact of NAC treatment as a strategy to improve mucus penetration (Takatsuka et al., 2006). The authors reported that treatment of rats with NAC led to an increased absorption of calcitonin, which was associated with mucosal and microvilli damage. However, it is to be noted that the mentioned study focuses on the intraintestinal application of NAC.

The use of mucus modulating agents like NAC to improve drug uptake by decreasing mucus barrier properties can be of advantage as it allows the application of simpler formulations. The improvement of mucus penetration in this scenario is achieved by the mucus modulating agent, applied prior to the use of the drug carrier. Such formulations can be realized by use of less complex and cheaper manufacturing processes (Nordgård and Draget, 2018), also resulting in lower costs for the development stage.

The data presented in this study emphasize that the application of mucus modulating strategies should be considered with caution, in particular if unintended exposure to particles is expected. In this context, a compromise should be made between the dose necessary to ensure the efficient delivery of the intended agent and the dose allowing for unintended penetration of environmental particles.

4. Conclusion

This study focuses on the impact of mucus modulation on the protective role of mucus taking into consideration the potential environmental/occupational exposure.

Differentiated Calu-3 cells as an *in vitro* mucus source have been characterized and a mucus modulation protocol involving the NAC nebulization that successfully enhanced NP transport through mucus has been developed. We demonstrated that Calu-3 cells provide a mucus layer of a thickness comparable to the human tracheal mucus, which protects the underlying cells and can successfully be employed for investigation of the protective role of mucus. We found that modulation of *in vitro* mucus *via* NAC significantly increased particle penetration and nanoparticle-induced cytotoxicity, indicating a reduced barrier capacity

of modulated mucus.

Our results suggest that assessment of the impact of mucus modulation on the protective role of mucus is essential for a successful development of therapy protocols involving mucus modulation as a strategy for enhancing drug carrier penetration through mucus.

Author contributions

E.M. and K.S. contributed equally to this work. E.M., M.S., A.K., designed the study. E.M. performed the characterization of microvilli formation and mucin secretion of cells. K.S. performed tight junction characterization, nanoparticle penetration and cytotoxicity experiments. E.M. and K.S. performed mucus thickness analysis. M.K. carried out electron microscopy. E.M., K.S., M.K., M.S., A.K., contributed to data analysis. E.M., K.S., M.S., and A.K. wrote the paper. All authors have given approval to the final version of the manuscript.

Funding sources

This research did not receive any specific grant from funding agencies in the public, commercial, or not-for-profit sectors.

Notes

The authors declare no competing financial interest.

Declaration of Competing Interest

The authors declare that they have no known competing financial interests or personal relationships that could have appeared to influence the work reported in this paper.

Data availability

Data will be made available on request.

Acknowledgments

The authors thank Anja Colbus for particle characterization and Hilal Ergül for immunostaining of samples showing mucin secretion. The authors thank Dr. Christiane Petzold for fruitful proofreading the manuscript.

Appendix A. Supplementary data

Supplementary data to this article can be found online at https://doi.org/10.1016/j.ijpx.2023.100212.

References

Aldini, G., Altomare, A., Baron, G., Vistoli, G., Carini, M., Borsani, L., Sergio, F., 2018. N-Acetylcysteine as an antioxidant and disulphide breaking agent: the reasons why. Free Radic. Res. 52, 751–762. https://doi.org/10.1080/10715762.2018.1468564.

Bansil, R., Turner, B.S., 2018. The biology of mucus: composition, synthesis and organization. Adv. Drug Deliv. Rev. 124, 3–15. https://doi.org/10.1016/j.addr.2017.09.023.

Berger, J.T., Voynow, J.A., Peters, K.W., Rose, M.C., 1999. Respiratory carcinoma cell lines: MUC genes and glycoconjugates. Am. J. Respir. Cell Mol. Biol. 20, 500–510.

Boegh, M., Baldursdottir, S.G., Nielsen, M.H., Müllertz, A., Nielsen, H.M., 2013. Development an rheological profiling of biosimilar mucus. Annu. Trans. Nord. Rheol. Soc. 21, 233–240.

Boucher, C.F., 2019. Muco-Obstructive Lung Diseases. N. Engl. J. Med. 380, 1941–1953. https://doi.org/10.1056/NEJMra1813799.

Braakhuis, H.M., Gremmer, E.R., Bannuscher, A., Drasler, B., Keshavan, S., Rothen-Rutishauser, B., Birk, B., Verlohner, A., Landsiedel, R., Meldrum, K., Doak, S.H., Clift, M.J.D., Erdem, J.S., Foss, O.A.H., Zienolddiny-Narui, S., Serchi, T., Moschini, E., Weber, P., Burla, S., Kumar, P., Schmid, O., Zwart, E., Vermeulen, J.P., Vandebriel, R.J., 2023. Transferability and reproducibility of exposed air-liquid interface co-culture lung models. NanoImpact 31, 100466. https://doi.org/10.1016/j.impact.2023.100466.

Bustamante-Marin, X.M., Ostrowski, L.E., 2017. Cilia and mucociliary clearance. Cold Spring Harb. Perspect. Biol. 9 https://doi.org/10.1101/cshperspect.a028241.

Button, B., Cai, L.-H., Ehre, C., Kesimer, M., Hill, D.B., Sheehan, J.K., Boucher, R.C., Rubinstein, M., 2012. A periciliary brush promotes the lung health by separating the mucus layer from airway epithelia. Science 337, 937–941. https://doi.org/10.1126/science.1223012.

Calverley, P., Rogliani, P., Papi, A., 2021. Safety of N-acetylcysteine at high doses in chronic respiratory diseases: a review. Drug Saf. 44, 273–290. https://doi.org/10.1007/s40264-020-01026-y.

Carlson, T.L., Lock, J.Y., Carrier, R.L., 2018. Engineering the mucus barrier. Annu. Rev. Biomed. Eng. 20, 197–220. https://doi.org/10.1146/annurev-bioeng-062117-121156.

Carvalho, T.C., Peters, J.I., Williams, R.O., 2011. Influence of particle size on regional lung deposition–what evidence is there? Int. J. Pharm. 406, 1–10. https://doi.org/10.1016/j.ijpharm.2010.12.040.

Chater, P.I., Wilcox, M.D., Pearson, J.P., 2018. Efficacy and safety concerns over the use of mucus modulating agents for drug delivery using nanoscale systems. Adv. Drug Deliv. Rev. 124, 184–192. https://doi.org/10.1016/j.addr.2017.12.006.

Dausend, J., Musyanovych, A., Dass, M., Walther, P., Schrezenmeier, H., Landfester, K., Mailänder, V., 2008. Uptake mechanism of oppositely charged fluorescent nanoparticles in HeLa cells. Macromol. Biosci. 8, 1135–1143. https://doi.org/10.1002/mabi.200800123.

Dekali, S., Gamez, C., Kortulewski, T., Blazy, K., Rat, P., Lacroix, G., 2014. Assessment of an in vitro model of pulmonary barrier to study the translocation of nanoparticles. Toxicol. Rep. 1, 157–171. https://doi.org/10.1016/j.toxrep.2014.03.003.

Ding, Y., Weindl, P., Lenz, A.G., Mayer, P., Krebs, T., Schmid, O., 2020. Quartz crystal microbalances (QCM) are suitable for real-time dosimetry in nanotoxicological studies using VITROCELL®Cloud cell exposure systems. Part. Fibre Toxicol. 17, 1–20. https://doi.org/10.1186/s12989-020-00376-w.

Ehre, C., Rushton, Z.L., Wang, B., Hothem, L.N., Morrison, C.B., Fontana, N.C., et al., 2019. An improved inhaled mucolytic to treat airway muco-obstructive diseases. Am. J. Respir. Crit. Care Med. 199 (2), 171–180. https://doi.org/10.1164/rccm.201802-0245OC.

Esther, C.R., Muhlebach, M.S., Ehre, C., Hill, D.B., Wolfgang, M.C., Kesimer, M., et al., 2019. Mucus accumulation in the lungs precedes structural changes and infection in children with cystic fibrosis. Sci. Transl. Med. 11 https://doi.org/10.1126/scitranslmed.aav3488 eaav3488.

Fiegel, J., Ehrhardt, C., Schaefer, U.F., Lehr, C.-M., Hanes, J., 2003. Large porous particle impingement on lung epithelial cell monolayers–toward improved particle characterization in the lung. Pharm. Res. 20, 788–796. https://doi.org/10.1023/A:1023441804464.

Florea, B.I., Cassara, M.L., Junginger, H.E., Borchard, G., 2003. Drug transport and metabolism characteristics of the human airway epithelial cell line Calu-3. J. Control. Release 87, 131–138. https://doi.org/10.1016/S0168-3659(02)00356-5.

Fogh, J., Fogh, J.M., Orfeo, T., 1977. One hundred and twenty-seven cultured human tumor cell lines producing tumors in nude mice. J. Natl. Cancer Inst. 59, 221–226. https://doi.org/10.1093/jnci/59.1.221.

Fröhlich, E., 2012. The role of surface charge in cellular uptake and cytotoxicity of medical nanoparticles. Intl. J. Nanomed. 7, 5577–5591. https://doi.org/10.2147/IJN.S36111.

Frye, R.E., Berk, M., 2018. The therapeutic use of N-acetylcysteine (NAC) in medicine. In: The Therapeutic Use of N-Acetylcysteine (NAC) in Medicine. https://doi.org/10.1007/978-981-10-5311-5.

Fu, Y., Fan, M., Xu, L., Wang, H., Hu, Q., Jin, Y., 2022. Amino-functionalized polystyrene nano-plastics induce mitochondria damage in human umbilical vein endothelial cells. Toxics. 10, 215. https://doi.org/10.3390/toxics 10050215.

Gamazo, C., Martin-Arbella, N., Brotons, A., Camacho, A.I., Irache, J.M., 2015. Mimicking microbial strategies for the design of mucus-permeating nanoparticles for oral immunization. Eur. J. Pharm. Biopharm. 96, 454–463. https://doi.org/10.1016/j.ejpb.2015.01.010.

Ghanem, R., Laurent, V., Roquefort, P., Haute, T., Ramel, S., Le Gall, T., Aubry, T., Montier, T., 2021. Optimizations of In Vitro Mucus and Cell Culture Models to Better Predict In Vivo Gene Transfer in Pathological Lung Respiratory Airways: Cystic Fibrosis as an Example. Pharmaceutics 13, 47. https://doi.org/10.3390/pharmaceutics13010047.

Grainger, C.I., Greenwell, L.L., Lockley, D.J., Martin, G.P., Forbes, B., 2006. Culture of Calu-3 cells at the air interface provides a representative model of the airway epithelial barrier. Pharm. Res. 23, 1482–1490. https://doi.org/10.1007/s11095-006-0255-0.

Gupta, R., Radicioni, G., Abdelwahab, S., Dang, H., Carpenter, J., Chua, M., Mieczkowski, P.A., Sheridan, J.T., Randell, S.H., Kesimer, M., 2019. Intercellular communication between airway epithelial cells is mediated by exosome-like vesicles. Am. J. Respir. Cell Mol. Biol. 60, 209–220. https://doi.org/10.1165/rcmb.2018-0156OC.

Haghi, M., Traini, D., Young, P., 2014. In vitro cell integrated impactor deposition methodology for the study of aerodynamically relevant size fractions from commercial pressurised metered dose inhalers. Pharm. Res. 31, 1779–1787. https://doi.org/10.1007/s11095-013-1282-2.

Hasegawa, Y., Mark Welch, J.L., Rossetti, B.J., Borisy, G.G., 2017. Preservation of three-dimensional spatial structure in the gut microbiome. PLoS One 12, e0188257. https://doi.org/10.1371/journal.pone.0188257.

Henderson, A.G., Ehre, C., Button, B., Abdullah, L.H., Cai, L.H., Leigh, M.W., DeMaria, G. C., Matsui, H., Donaldson, S.H., Davis, C.W., Sheehan, J.K., Boucher, R.C., Kesimer, M., 2014. Cystic fibrosis airway secretions exhibit mucin hyperconcentration and increased osmotic pressure. J. Clin. Invest. 124, 3047–3060. https://doi.org/10.1172/JCI73469.

Hill, D.B., Vasquez, P.A., Mellnik, J., McKinley, S.A., Vose, A., Mu, F., Henderson, A.G., Donaldson, S.H., Alexis, N.E., Boucher, R.C., Forest, M.G., 2014. A Biophysical Basis for Mucus Solids Concentration as a Candidate Biomarker for Airways Disease. PLOS One 9, e87681. https://doi.org/10.1371/journal.pone.0087681.

Huck, B.C., Hartwig, O., Biehl, A., Schwarzkopf, K., Wagner, C., Loretz, B., Murgia, X., Lehr, C.-M., 2019. Macro- and microrheological properties of mucus surrogates in comparison to native intestinal and pulmonary mucus. Biomacromolecules 20, 3504–3512. https://doi.org/10.1021/acs.biomac.9b00780.

Jachak, A., Lai, S.K., Hida, K., Suk, J.S., Markovic, N., Biswal, S., Breysse, P.N., Hanes, J., 2012. Transport of metal oxide nanoparticles and single-walled carbon nanotubes in human mucus. Nanotoxicology 6, 614–622. https://doi.org/10.3109/17435390.2011.598244.

Juntke, J., Murgia, X., Günday Türeli, N., Türeli, A.E., Thorn, C.R., Schneider, M., Schneider-Daum, N., de Souza Carvalho-Wodarz, C., Lehr, C.-M., 2021. Testing of aerosolized ciprofloxacin nanocarriers on cystic fibrosis airway cells infected with P. aeruginosa biofilms. Drug Deliv. Transl. Res. https://doi.org/10.1007/s13346-021-01002-8.

Kik, K., Bukowska, B., Sicińska, P., 2020. Polystyrene nanoparticles: sources, occurrence in the environment, distribution in tissues, accumulation and toxicity to various organisms. Environ. Pollut. 262, 114297. https://doi.org/10.1016/j.envpol.2020.114297.

Kirch, J., Schneider, A., Abou, B., Hopf, A., Schaefer, U.F., Schneider, M., et al., 2012. Optical tweezers reveal relationship between microstructure and nanoparticle penetration of pulmonary mucus. Proc. Natl. Acad. Sci. 109 (45), 18355–18360. https://doi.org/10.1073/pnas.1214066109.

Kreda, S.M., Okada, S.F., Van Heusden, C.A., O'Neal, W., Gabriel, S., Abdullah, L., Davis, C.W., Boucher, R.C., Lazarowski, E.R., 2007. Coordinated release of nucleotides and mucin from human airway epithelial Calu-3 cells. J. Physiol. 584, 245–259. https://doi.org/10.1113/jphysiol.2007.139840.

Kreft, M.E., Jerman, U.D., Lasič, E., Hevir-Kene, N., Rižner, T.L., Peternel, L., Kristan, K., 2015. The characterization of the human cell line Calu-3 under different culture conditions and its use as an optimized in vitro model to investigate bronchial epithelial function. Eur. J. Pharm. Sci. 69, 1–9. https://doi.org/10.1016/j.ejps.2014.12.017.

Lababidi, N., Ofosu Kissi, E., Elgaher, W.A.M., Sigal, V., Haupenthal, J., Schwarz, B.C., Hirsch, A.K.H., Rades, T., Schneider, M., 2019. Spray-drying of inhalable, multifunctional formulations for the treatment of biofilms formed in cystic fibrosis. J. Control. Release 314, 62–71. https://doi.org/10.1016/J.JCONREL.2019.10.038.

Lababidi, N., Montefusco-Pereira, C.V., de Souza Carvalho-Wodarz, C., Lehr, C.M., Schneider, M., 2020. Spray-dried multidrug particles for pulmonary co-delivery of antibiotics with N-acetylcysteine and curcumin-loaded PLGA-nanoparticles. Eur. J. Pharm. Biopharm. 157, 200–210. https://doi.org/10.1016/J.EJPB.2020.10.010.

Lee, D.F., Lethem, M.I., Lansley, A.B., 2021. A comparison of three mucus-secreting airway cell lines (Calu-3, SPOC1 and UNCN3T) for use as biopharmaceutical models of the nose and lung. Eur. J. Pharm. Biopharm. 167, 159–174. https://doi.org/10.1016/j.ejpb.2021.07.016.

Li, X., Kang, B., Eom, Y., Zhong, J., Lee, H.K., Kim, H.M., Song, J.S., 2022. Comparison of cytotoxicity effects induced by four different types of nanoparticles in human corneal and conjunctival epithelial cells. Sci. Rep. 12, 155. https://doi.org/10.1038/s41598-021-04199-3.

Lillehoj, E.P., Kato, K., Lu, W., Kim, K.C., 2013. Cellular and Molecular Biology of Airway Mucins, International Review of Cell and Molecular Biology. Elsevier. https://doi.org/10.1016/B978-0-12-407697-6.00004-0.

Lodes, N., Seidensticker, K., Perniss, A., Nietzer, S., Oberwinkler, H., May, T., Walles, T., Hebestreit, H., Hackenberg, S., Steinke, M., 2020. Investigation on ciliary functionality of HaCaT keratinocytes response on antimicrobial atelocollagen substrates: extent of cytotoxicity, cell viability and proliferation different airway epithelial cell lines in three-dimensional cell culture. Tissue Eng. - Part A 26, 432–440. https://doi.org/10.1089/ten.tea.2019.0188.

López-García, J., Lehocký, M., Humpolíček, P., Sáha, P., 2014. J. Funct. Biomater. 5, 43–57. https://doi.org/10.3390/jfb5020043.

Meindl, C., Stranzinger, S., Dzidic, N., Salar-Behzadi, S., Mohr, S., Zimmer, A., Fröhlich, E., 2015. Permeation of therapeutic drugs in different formulations across the airway epithelium in vitro. PLoS One 10, 1–19. https://doi.org/10.1371/journal.pone.0135690.

Meziu, E., Koch, M., Fleddermann, J., Schwarzkopf, K., Schneider, M., Kraegeloh, A., 2021. Visualization of the structure of native human pulmonary mucus. Int. J. Pharm. 597, 120238. https://doi.org/10.1016/j.ijpharm.2021.120238.

Morrison, C.B., Markovetz, M.R., Ehre, C., 2019. Mucus, mucins, and cystic fibrosis. Pediatr. Pulmonol. 54, S84–S96. https://doi.org/10.1002/ppul.24530.

Mura, S., Hillaireau, H., Nicolas, J., Kerdine-Römer, S., Le Droumaguet, B., Deloménie, C., Nicolas, V., Pallardy, M., Tsapis, N., Fattal, E., 2011. Biodegradable nanoparticles meet the bronchial airway barrier: how surface properties affect their interaction with mucus and epithelial cells. Biomacromolecules 12, 4136–4143. https://doi.org/10.1021/bm201226x.

Murgia, X., Pawelzyk, P., Schaefer, U.F., Wagner, C., Willenbacher, N., Lehr, C.M., 2016. Size-limited penetration of nanoparticles into porcine respiratory mucus after aerosol deposition. Biomacromolecules 17, 1536–1542. https://doi.org/10.1021/acs.biomac.6b00164.

Murgia, X., Loretz, B., Hartwig, O., Hittinger, M., Lehr, C., 2018. The role of mucus on drug transport and its potential to affect therapeutic outcomes. Adv. Drug Deliv. Rev. 124, 82–97. https://doi.org/10.1016/j.addr.2017.10.009.

Nafee, N., Forier, K., Braeckmans, K., Schneider, M., 2018. Mucus-penetrating solid lipid nanoparticles for the treatment of cystic fibrosis: Proof of concept, challenges and pitfalls. Eur. J. Pharm. Biopharm. 124, 125–137. https://doi.org/10.1016/j.ejpb.2017.12.017.

Najahi-Missaoui, W., Arnold, R.D., Cummings, B.S., 2021. Safe nanoparticles: are we there yet? Int. J. Mol. Sci. 22, 1–22. https://doi.org/10.3390/ijms22010385.

Nordgård, C.T., Draget, K.I., 2018. Co association of mucus modulating agents and nanoparticles for mucosal drug delivery. Adv. Drug Deliv. Rev. 124, 175–183. https://doi.org/10.1016/j.addr.2018.01.001.

Osinka, A., Poprzeczko, M., Zielinska, M.M., Fabczak, H., Joachimiak, E., Wloga, D., 2019. Ciliary proteins: filling the gaps. recent advances in deciphering the protein composition of motile ciliary complexes. Cells 8, 730. https://doi.org/10.3390/cells8070730.

Patton, J.S., 1996. Mechanisms of macromolecule absorption by the lungs. Adv. Drug Deliv. Rev. 19, 3–36. https://doi.org/10.1016/0169-409X(95)00113-L.

Peng, K., Gao, Y., Angsantikul, P., LaBarbiera, A., Goetz, M., Curreri, A.M., Rodrigues, D., Tanner, E.E.L., Mitragotri, S., 2021. Modulation of gastrointestinal mucus properties with ionic liquids for drug delivery. Adv. Healthc. Mater. 10, 1–14. https://doi.org/10.1002/adhm.202002192.

Sadowska, A.M., 2012. N-Acetylcysteine mucolysis in the management of chronic obstructive pulmonary disease. Ther. Adv. Respir. Dis. 6, 127–135. https://doi.org/10.1177/1753465812437563.

Song, D., Iverson, E., Kaler, L., Boboltz, A., Scull, M.A., Duncan, G.A., 2022. MUC5B mobilizes and MUC5AC spatially aligns mucociliary transport on human airway epithelium. Sci. Adv. 8, eabq5049. https://doi.org/10.1126/sciadv.abq5049.

Sonntag, T., Rapp, M., Didier, P., Lebeau, L., Pons, F., Casset, A., 2022. Mucus-producing epithelial models for investigating the activity of gene delivery systems in the lung. Int. J. Pharm. 614, 121423. https://doi.org/10.1016/J.IJPHARM.2021.121423.

Stentebjerg-Andersen, A., Notlevsen, I.V., Brodin, B., Nielsen, C.U., 2011. Calu-3 cells grown under AIC and LCC conditions: implications for dipeptide uptake and transepithelial transport of substances. Eur. J. Pharm. Biopharm. 78, 19–26. https://doi.org/10.1016/j.ejpb.2010.12.030.

Suk, J.S., Boylan, N.J., Trehan, K., Tang, B.C., Schneider, C.S., Lin, J.M.G., Boyle, M.P., Zeitlin, P.L., Lai, S.K., Cooper, M.J., Hanes, J., 2011a. N-acetylcysteine enhances cystic fibrosis sputum penetration and airway gene transfer by highly compacted DNA nanoparticles. Mol. Ther. 19, 1981–1989. https://doi.org/10.1038/mt.2011.160.

Suk, J.S., Lai, S.K., Boylan, N.J., Dawson, M.R., Boyle, M.P., Hanes, J., 2011b. Rapid transport of muco-inert nanoparticles in cystic fibrosis sputum treated with *N* -acetyl cysteine. Nanomedicine 6, 365–375. https://doi.org/10.2217/nnm.10.123.

Takatsuka, S., Morita, T., Koguchi, A., Horikiri, Y., Yamahara, H., Yoshino, H., 2006. Synergistic absorption enhancement of salmon calcitonin and reversible mucosal injury by applying a mucolytic agent and a non-ionic surfactant. Int. J. Pharm. 316, 124–130. https://doi.org/10.1016/j.ijpharm.2006.02.053.

Tilney, L.G., Connelly, P.S., Guild, G.M., 2004. Microvilli appear to represent the first step in actin bundle formation in Drosophila bristles. J. Cell Sci. 117, 3531–3538. https://doi.org/10.1242/jcs.01215.

Tseng, H.-Y., Lin, H.-L., Chiang, H.-S., 2022. In vitro evaluation of aerosol delivery by hand-held mesh nebulizers in an adult spontaneous breathing lung model. J. Aerosol. Med. Pulm. Drug Deliv. 35, 83–90. https://doi.org/10.1089/jamp.2021.0010.

Vethaak, A.D., Legler, J., 2021. Microplastics and human health. Science 371, 672–674. https://doi.org/10.1126/science.abe5041.

Vukosavljevic, B., Murgia, X., Schwarzkopf, K., Schaefer, U.F., Lehr, C., Windbergs, M., 2017. Tracing molecular and structural changes upon mucolysis with N-acetyl cysteine in human airway mucus. Int. J. Pharm. 533, 373–376. https://doi.org/10.1016/j.ijpharm.2017.07.022.

Walczak, A.P., Kramer, E., Hendriksen, P.J.M., Tromp, P., Helsper, J.P.F.G., van der Zande, M., Rietjens, I.M.C.M., Bouwmeester, H., 2015. Translocation of differently sized and charged polystyrene nanoparticles in in vitro intestinal cell models of increasing complexity. Nanotoxicology 9, 453–461. https://doi.org/10.3109/17435390.2014.944599.

Wan, H., Winton, H.L., Soeller, C., Stewart, G.A., Thompson, P.J., Gruenert, D.C., Cannell, M.B., Garrod, D.R., Robinson, C., 2000. Tight junction properties of the immortalized human bronchial epithelial cell lines Calu-3 anmd 16HBE14o. Eur. Respir. J. 15, 1058–1068. https://doi.org/10.1034/j.1399-3003.2000.01514.x.

Wang, Y.Y., Lai, S.K., So, C., Schneider, C., Cone, R., Hanes, J., 2011. Mucoadhesive nanoparticles may disrupt the protective human mucus barrier by altering its microstructure. PLoS One 6, 1–7. https://doi.org/10.1371/journal.pone.0021547.

Wang, T., Wang, Lu, Li, X., Hu, X., Han, Y., Luo, Y., Wang, Z., Li, Q., Aldalbahi, A., Wang, Lihua, Song, S., Fan, C., Zhao, Y., Wang, M., Chen, N., 2017. Size-dependent regulation of intracellular trafficking of polystyrene nanoparticle-based drug-delivery systems. ACS Appl. Mater. Interfaces 9, 18619–18625. https://doi.org/10.1021/acsami.7b05383.

Wine, J.J., 1999. The genesis of cystic fibrosis lung disease. J. Clin. Invest. 103, 309–312. https://doi.org/10.1172/JCI6222.

Wu, T., Täubel, M., Holopainen, R., Viitanen, A.K., Vainiotalo, S., Tuomi, T., Keskinen, J., Hyvärinen, A., Hämeri, K., Saari, S.E., Boor, B.E., 2018. Infant and Adult Inhalation Exposure to Resuspended Biological Particulate Matter. Environ. Sci. Technol. 52, 237–247. https://doi.org/10.1021/acs.est.7b04183.

Xia, W., Wang, Y., Chen, S., Huang, J., Wang, B., Zhang, G.J., Zhang, Y., Liu, X., Ma, J., Gong, P., Jiang, Y., Wu, M., Xue, J., Wei, L., Zhang, T., 2022. Double trouble of Air Pollution by Anthropogenic Dust. Environ. Sci. Technol. 56, 761–769. https://doi.org/10.1021/acs.est.1c04779.